National Conference with International Participation

ENGINEERING MECHANICS 2008

Svratka, Czech Republic, May 12 – 15, 2008

NUMERICAL AND EXPERIMENTAL INVESTIGATION OF TRANSONIC FLOW THROUGH 2-D MODEL OF CLEARANCE GAP

J. Vimmr[*], O. Bublík, M. Luxa[**], R. Dvořák, D. Šimurda

Summary: *The main objective of the study presented here is to compare the results obtained from numerical simulations and experimental measurements of the transonic flow through the 2-D model of the male rotor-housing gap in a dry screw compressor for several clearance throat dimensions and pressure ratios. With regard to the numerical investigation, a compressible Navier-Stokes solver has been developed for the purpose of clearance flow modelling. The presented numerical solver is based on the cell-centred finite volume method defined on structured quadrilateral grids. For the spacial discretization of the inviscid part of the numerical flux, the AUSM scheme with a β-version of the minmod limiter is applied. For the time integration, the two stage second order Runge-Kutta algorithm is used. Concerning the experimental measurements, the Schlieren method in Toepler configuration was carried out.*

1. Introduction

Mathematical modelling and experimental investigation of transonic flow in very narrow channels and gaps is one of the topical and demanding problems of internal aerodynamics. Clearance gaps in screw compressors represent one of many applications. Some experimental and numerical simulations of gas flow through a 2-D model of the male rotor-housing gap (the sealing gap between the head of the male rotor tooth and the screw compressor housing) have been already presented (Kauder et al., 2000). All numerical computations introduced in this study were performed by CFD package Fluent.

In (Vimmr, 2004), the early numerical results, which were obtained using a compressible Navier-Stokes solver for the case of the laminar clearance flow computation performed for the given pressure ratio $p_2/p_{01} = 0.5$ through the 2-D model of the male rotor-housing gap with the throat dimension of 100 μm, were published. The numerical solver developed by one of the authors was based on the cell-centred finite volume formulation of the central explicit two-step TVD MacCormack scheme proposed by Causon (1989) for a structured quadrilateral grid.

[*] Ing. Jan Vimmr, Ph.D., Ing. Ondřej Bublík: Department of Mechanics, Faculty of Applied Sciences, University of West Bohemia, Univerzitní 22; 306 14 Plzeň; tel.: +420 377 632 314, fax: +420 377 632 302; e-mail: jvimmr@kme.zcu.cz

[**] Ing. Martin Luxa, Ph.D., Ing. Rudolf Dvořák, DrSc., Ing. David Šimurda: Institute of Thermomechanics, Academy of Sciences of the Czech Republic, Dolejškova 1402/5; 182 02 Praha 8; tel.: +420 266 053 352, fax: +420 286 584 695; e-mail: luxa@it.cas.cz

Regarding the mentioned 2-D model of the male rotor-housing gap, new optical measurements were carried out by Luxa et al. (2008) using the Schlieren method in Toepler configuration. The obtained experimental results show that the occurrence of shock waves in the supersonic region of the considered 2-D model of the clearance gap is dependent on its throat dimension H and on the pressure ratio p_2/p_{01}.

Therefore, the research attention of this study is focused on the numerical solution of a laminar compressible viscous fluid flow through the 2-D model of the male rotor-housing gap for three different throat dimensions (200 µm, 350 µm and 500 µm) and for selected pressure ratios ($p_2/p_{01} = 0.2$, $p_2/p_{01} = 0.182$ and $p_2/p_{01} = 0.183$) with atmospheric pressure at the inlet. All numerical results presented here are qualitatively compared with the experimental results, which were obtained for the same gap geometry and for the same flow conditions. The numerical simulations were performed by a numerical solver based on the cell-centred finite volume method defined on structured quadrilateral grids. The numerical code is developed to solve the actual transonic flow problems in very narrow channels and gaps. For the spacial discretization of the inviscid part of the numerical flux, the AUSM flux vector splitting scheme proposed by Liou & Steffen (1993) is applied. The first order spatial accuracy of the AUSM scheme is improved to the second order by a linear reconstruction with a β-version of the minmod limiter proposed by the authors. The viscous part of the numerical flux is modelled using a finite volume version of central differences on dual cells. For the time integration, we use the two stage second order Runge-Kutta algorithm.

2. Problem formulation

The clearance flow can be reasonably simulated by the computational fluid dynamics (CFD) for so called dry compressors, Fig. 1 (left), where no multiphase flow occurs. The male rotor-housing gap in a dry screw compressor is modelled in a screw compressor frontal cross-section (the plane perpendicular to rotors axes), Fig. 1 (right), in the form of a two-dimensional computational domain $\Omega \subset R^2$, Fig. 2. It is bounded by two adiabatic impermeable walls $\partial\Omega_W = \partial\Omega_{WS} \cup \partial\Omega_{WR}$ that corresponds to the circular part of the screw compressor housing $\partial\Omega_{WS}$ and to the head of the male rotor tooth $\partial\Omega_{WR}$. The other boundaries of the computational domain Ω represent the inlet $\partial\Omega_1$ from the higher pressure chamber and the outlet $\partial\Omega_2$ to the lower pressure screw compressor chamber, Fig. 2. It is assumed that the male rotor does not move. Hence, the influence of the male rotor motion is not investigated.

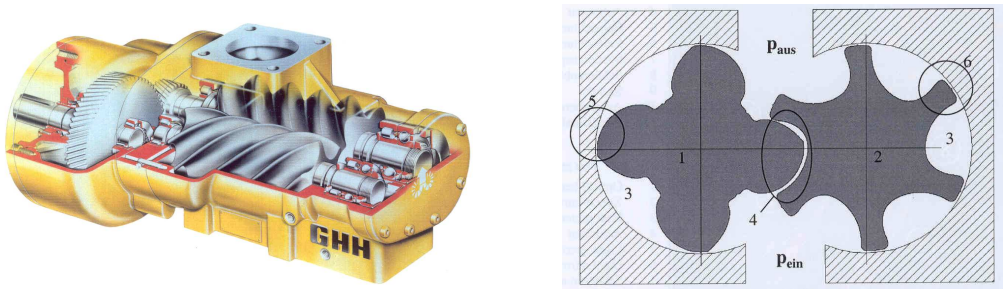

Fig. 1: Dry screw compressor (left). Screw compressor frontal cross-section (right): 1 – male rotor, 2 – female rotor, 5 – male rotor-housing gap (considered clearance gap)

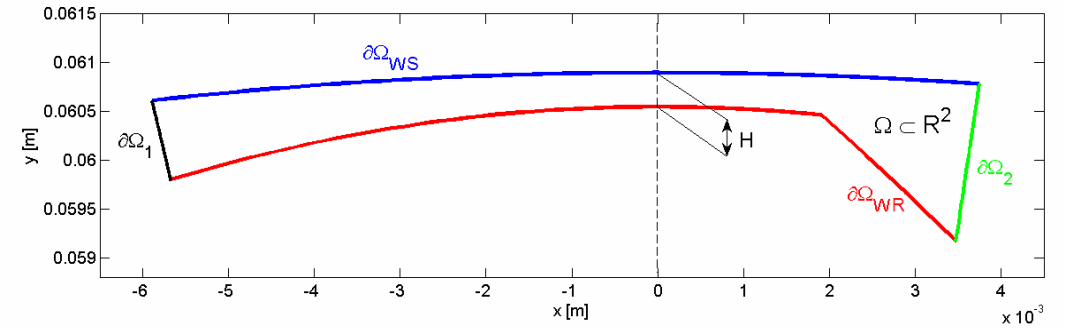

Fig. 2: 2-D computational domain $\Omega \subset R^2$ with the boundary $\partial\Omega = \partial\Omega_1 \cup \partial\Omega_2 \cup \partial\Omega_W$

Let H be the throat dimension, i.e. the width of the 2-D clearance gap in its narrowest section for $x = 0$, Fig. 2. The clearance flow is studied for three different throat dimensions ($H_1 = 200$ µm, $H_2 = 350$ µm and $H_3 = 500$ µm) and for selected pressure ratios ($p_2/p_{01} = 0.2$, $p_2/p_{01} = 0.182$ and $p_2/p_{01} = 0.183$) with atmospheric pressure at the inlet. In this study, four cases are tested numerically and experimentally.

For the ***test case A*** ($H_2 = 350$ µm, $p_2/p_{01} = 0.2$), the reference Reynolds number $Re_{ref} = \rho_{ref} u_{ref} H_{2ref} / \eta_{ref} = 6449$ was computed from selected reference values $p_{ref} \equiv p_{01} = 101325$ Pa, $T_{ref} \equiv T_{01} = 298.15$ K, $H_{2ref} \equiv H_2 = 3.5 \cdot 10^{-4}$ m, $r_{ref} \equiv r = 287$ J/(kg K) and $\eta_{ref} \equiv \eta = 1.879 \cdot 10^{-5}$ kg/(m s) leading to $\rho_{ref} = p_{ref}/(r_{ref} T_{ref}) = 1.184$ kg/m^3 and $u_{ref} = \sqrt{p_{ref}/\rho_{ref}} = 292.52$ m/s.

For the ***test case B*** ($H_3 = 500$ µm, $p_2/p_{01} = 0.183$), the reference Reynolds number $Re_{ref} = \rho_{ref} u_{ref} H_{3ref} / \eta_{ref} = 9213$ was computed from selected reference values $p_{ref} \equiv p_{01} = 101325$ Pa, $T_{ref} \equiv T_{01} = 298.15$ K, $H_{3ref} \equiv H_3 = 5 \cdot 10^{-4}$ m, $r_{ref} \equiv r = 287$ J/(kg K) and $\eta_{ref} \equiv \eta = 1.879 \cdot 10^{-5}$ kg/(m s) leading to $\rho_{ref} = p_{ref}/(r_{ref} T_{ref}) = 1.184$ kg/m^3 and $u_{ref} = \sqrt{p_{ref}/\rho_{ref}} = 292.52$ m/s.

For the ***test case C*** ($H_1 = 200$ µm, $p_2/p_{01} = 0.182$), the reference Reynolds number $Re_{ref} = \rho_{ref} u_{ref} H_{1ref} / \eta_{ref} = 3685$ was computed from selected reference values $p_{ref} \equiv p_{01} = 101325$ Pa, $T_{ref} \equiv T_{01} = 298.15$ K, $H_{1ref} \equiv H_1 = 2 \cdot 10^{-4}$ m, $r_{ref} \equiv r = 287$ J/(kg K) and $\eta_{ref} \equiv \eta = 1.879 \cdot 10^{-5}$ kg/(m s) leading to $\rho_{ref} = p_{ref}/(r_{ref} T_{ref}) = 1.184$ kg/m^3 and $u_{ref} = \sqrt{p_{ref}/\rho_{ref}} = 292.52$ m/s.

3. Governing equations for laminar compressible fluid flow

Because of relatively low values of the reference Reynolds numbers Re_{ref} in the considered ***test cases A – C*** of the clearance flow through the 2-D models of the male rotor-housing gap with different throat dimensions H mentioned above, the laminar flow model described by

the non-linear conservative system of the two-dimensional compressible Navier-Stokes (NS) equations is assumed for our numerical computations.

Making an orientation calculation of the Knudsen number Kn using $Kn = (M/Re_{ref})\sqrt{\kappa\pi/2}$, see Karniadakis et al. (2005), the obtained values for all our computations are always lower than $Kn < 6 \cdot 10^{-4}$. Therefore, the fluid can still be considered as a continuum and the application of the complete non-linear system of the compressible NS equations for laminar heat-conducting, Newtonian fluid flow in an absolute frame of reference is acceptable. In non-dimensional conservative flux vector form, the governing equations are written for 2-D flow problems as

$$\frac{\partial \boldsymbol{w}}{\partial t} + \frac{\partial \boldsymbol{f}(\boldsymbol{w})}{\partial x} + \frac{\partial \boldsymbol{g}(\boldsymbol{w})}{\partial y} = \frac{1}{Re_{ref}}\left(\frac{\partial \boldsymbol{f}_V(\boldsymbol{w})}{\partial x} + \frac{\partial \boldsymbol{g}_V(\boldsymbol{w})}{\partial y} \right) \qquad \text{in} \quad \Omega_T = \Omega \times (0, T_N), \tag{1}$$

where Ω_T is the space time cylinder and $(0, T_N)$ is a time interval, $T_N > 0$. The column vector $\boldsymbol{w}(\boldsymbol{y}, t)$ of conservative flow variables and the Cartesian components $\boldsymbol{f}(\boldsymbol{w})$, $\boldsymbol{g}(\boldsymbol{w})$ of the total inviscid flux and $\boldsymbol{f}_V(\boldsymbol{w})$, $\boldsymbol{g}_V(\boldsymbol{w})$ of the total viscous flux are defined as

$$\boldsymbol{w} = \boldsymbol{w}(\boldsymbol{y}, t) = (\rho, \rho u, \rho v, E)^T \in R^4, \quad \boldsymbol{y} = (x, y)^T \in \Omega, \quad t \in (0, T_N), \tag{2}$$

$$\boldsymbol{f} = \boldsymbol{f}(\boldsymbol{w}) = (\rho u, \rho u^2 + p, \rho uv, (E + p)u)^T, \tag{3}$$

$$\boldsymbol{g} = \boldsymbol{g}(\boldsymbol{w}) = (\rho v, \rho uv, \rho v^2 + p, (E + p)v)^T, \tag{4}$$

$$\boldsymbol{f}_V = \boldsymbol{f}_V(\boldsymbol{w}) = (0, \tau_{xx}, \tau_{xy}, u\tau_{xx} + v\tau_{xy} - q_x)^T, \tag{5}$$

$$\boldsymbol{g}_V = \boldsymbol{g}_V(\boldsymbol{w}) = (0, \tau_{yx}, \tau_{yy}, u\tau_{yx} + v\tau_{yy} - q_y)^T. \tag{6}$$

In the above, ρ is the fluid density, p is the static pressure, E is the total energy per unit volume, u, v are the Cartesian components of the velocity vector $\boldsymbol{v} = (u, v)^T$, τ_{xx}, τ_{xy}, τ_{yx}, τ_{yy} are the laminar shear stresses and q_x, q_y are the heat flux terms given for a Newtonian fluid, (Hirsch, 1990). The external volume forces are not considered in all our test cases.

In this study, we assume the compressible fluid to be a perfect gas, even if the viscous effects are taken into account. From the ideal gas equation of state, the static pressure p is used to close the system of the compressible NS equations (1) as follows

$$p = \rho\, rT = (\kappa - 1)\left[E - \frac{1}{2}\rho(u^2 + v^2) \right], \tag{7}$$

where T is the thermodynamic temperature, $r = c_p - c_v$ is the gas constant per unit of mass, c_p and c_v are the specific heat coefficients under constant pressure and constant volume, respectively, and $\kappa = 1.4$ is the Poisson's constant (the ratio of specific heat coefficients c_p and c_v). The laminar Prandtl number Pr is defined for the perfect gas as $Pr = c_p \eta / k = 0.72$, where η is the molecular viscosity and k is the thermal conductivity.

4. Numerical method

For the discretization of the conservative system of the NS equations (1), the cell-centred finite volume method (FVM) on a structured quadrilateral grid was used. In the FVM, the bounded computational domain $\Omega \subset R^2$ is subdivided into a finite number of non-overlapping quadrilateral finite volumes Ω_{ij} with the boundary $\partial\Omega_{ij}$. Integrating the equation (1) over each control volume Ω_{ij} and applying the Gauss-Ostrogradski's Theorem, the following integral form is obtained

$$\frac{\partial}{\partial t}\int_{\Omega_{ij}} \boldsymbol{w}\,\mathrm{d}\Omega_{ij} + \oint_{\partial\Omega_{ij}} (n_x \boldsymbol{f} + n_y \boldsymbol{g})\,\mathrm{d}S = \frac{1}{Re_{ref}} \oint_{\partial\Omega_{ij}} (n_x \boldsymbol{f}_V + n_y \boldsymbol{g}_V)\,\mathrm{d}S\,, \tag{8}$$

where n_x and n_y are the Cartesian components of the outward unit vector normal to the differential surface $\mathrm{d}S$ of the control volume boundary $\partial\Omega_{ij}$. Substituting the first integral on the left side of equation (8) by $\boldsymbol{w}_{ij}\,|\Omega_{ij}|$, where $\boldsymbol{w}_{ij}$ is the numerical solution stored at the cell centroids (integral average of $\boldsymbol{w}$ over the control volume Ω_{ij}) and $|\Omega_{ij}|$ is the area of the cell Ω_{ij}, we get

$$\frac{\mathrm{d}\boldsymbol{w}_{ij}}{\mathrm{d}t}\,|\Omega_{ij}| + \oint_{\partial\Omega_{ij}} (n_x \boldsymbol{f} + n_y \boldsymbol{g})\,\mathrm{d}S = \frac{1}{Re_{ref}} \oint_{\partial\Omega_{ij}} (n_x \boldsymbol{f}_V + n_y \boldsymbol{g}_V)\,\mathrm{d}S\,. \tag{9}$$

The integrals in equation (9) can be approximated by a sum of numerical fluxes and equation (9) is rewritten in the following semidiscretized form on a quadrilateral control volume Ω_{ij} as

$$\frac{\mathrm{d}\boldsymbol{w}_{ij}}{\mathrm{d}t} = -\frac{1}{|\Omega_{ij}|}\left(\sum_{m=1}^{4} \boldsymbol{F}_m^I S_m - \frac{1}{Re_{ref}}\sum_{m=1}^{4} \boldsymbol{F}_m^V S_m\right), \tag{10}$$

where $\boldsymbol{F}_m^I$ and $\boldsymbol{F}_m^V$ are numerical inviscid and viscous fluxes, respectively, and act through the m-th edge of the quadrilateral control volume Ω_{ij}. We denote $S_m, m = 1,\ldots,4$ as the length of the m-th cell edge.

The approximation of the inviscid numerical fluxes $\boldsymbol{F}_m^I$ normal to the m-th edge ($m = 1,\ldots,4$) of the quadrilateral control volume Ω_{ij} was performed using the AUSM (**A**dvection **U**pstream **S**plitting **M**ethod) algorithm proposed by Liou & Steffen (1993). The inviscid numerical flux vector $\boldsymbol{F}^I$ consists of two physically distinct parts, namely convective and pressure terms

$$\boldsymbol{F}^I = n_x \boldsymbol{f} + n_y \boldsymbol{g} = V_n \begin{pmatrix} \rho \\ \rho u \\ \rho v \\ \rho H \end{pmatrix} + p \begin{pmatrix} 0 \\ n_x \\ n_y \\ 0 \end{pmatrix} = \hat{\boldsymbol{F}}^c + p \begin{pmatrix} 0 \\ n_x \\ n_y \\ 0 \end{pmatrix}, \tag{11}$$

where $H = E + p/\rho$ is the enthalpy, $V_n = u n_x + v n_y = \boldsymbol{v}^T \cdot \boldsymbol{n}$ is the convective velocity normal to the appropriate cell interface and $\hat{\boldsymbol{F}}^c$ denotes the convective part of the inviscid numerical flux. For each edge dividing two cells in the computational grid, we define the normal Mach

numbers for the left (L) and right (R) cells as $M_{nL} = V_{nL}/a_L$ and $M_{nR} = V_{nR}/a_R$, where a_L and a_R are values of the local speed of sound in the left and right cells, respectively. The interface convective Mach number $M_{L/R}$ is then determined by using Mach number splitting functions ($\mathrm{M}^{\pm}$) based on neighbouring normal Mach numbers

$$M_{L/R} = \mathrm{M}^{+}(M_{nL}) + \mathrm{M}^{-}(M_{nR}), \tag{12}$$

where the Mach number splitting functions are defined in the following way, (Liou, 1996),

$$\mathrm{M}^{\pm}(M) = \begin{cases} \dfrac{1}{2}(M \pm |M|), & \text{if} \quad |M| > 1, \\ \pm\dfrac{1}{4}(M \pm 1)^2 \pm \dfrac{1}{8}(M^2 - 1)^2, & \text{otherwise.} \end{cases} \tag{13}$$

Similarly, the interface pressure $p_{L/R}$ is obtained with contributions from the left and right cells using pressure splitting functions ($\mathrm{P}^{\pm}$) based on neighbouring normal Mach numbers

$$p_{L/R} = \mathrm{P}^{+}(M_{nL}) \cdot p_L + \mathrm{P}^{-}(M_{nR}) \cdot p_R, \tag{14}$$

where p_L and p_R are values of the static pressure in the left and right cells, respectively. The pressure splitting functions $\mathrm{P}^{\pm}$ are, (Liou, 1996),

$$\mathrm{P}^{\pm}(M) = \begin{cases} \dfrac{1}{2}(1 \pm \mathrm{sign}\,|M|), & \text{if} \quad |M| > 1, \\ \dfrac{1}{4}(M \pm 1)^2(2 \mp M), & \text{otherwise.} \end{cases} \tag{15}$$

Consequently, the convective term of the numerical flux through a cell interface can be effectively written as

$$\hat{\boldsymbol{F}}^{c}_{L/R} = \begin{cases} M_{L/R}\ \tilde{\boldsymbol{F}}^{c}_{R}, & \text{if} \quad M_{L/R} \le 0, \\ M_{L/R}\ \tilde{\boldsymbol{F}}^{c}_{L}, & \text{if} \quad M_{L/R} > 0, \end{cases} \qquad \text{where} \quad \tilde{\boldsymbol{F}}^{c}_{L(R)} = \begin{pmatrix} \rho a \\ \rho u a \\ \rho v a \\ \rho H a \end{pmatrix}_{L(R)}. \tag{16}$$

The total inviscid AUSM numerical flux through the m-th cell edge of the control volume Ω_{ij} can be finally expressed as

$$\boldsymbol{F}^{I}_{m} \equiv \boldsymbol{F}^{AUSM}_{L/R}(\boldsymbol{w}_L, \boldsymbol{w}_R) = \frac{1}{2} M_{L/R}(\tilde{\boldsymbol{F}}^{c}_{L} + \tilde{\boldsymbol{F}}^{c}_{R}) - \frac{1}{2} |M_{L/R}| (\tilde{\boldsymbol{F}}^{c}_{R} - \tilde{\boldsymbol{F}}^{c}_{L}) + p_{L/R} \begin{pmatrix} 0 \\ n_x \\ n_y \\ 0 \end{pmatrix}. \tag{17}$$

It is well known that upwind schemes in general are of the first order accuracy in space. Hence, the first order spatial accuracy of the AUSM scheme is improved to the second order by a linear reconstruction with a limiter. ***The linear reconstruction*** at each control volume of the structured quadrilateral grid is built in two independent directions. We assume that the neighbouring cells dimensions are comparable. Therefore, we do not perform the coordinates

transformation from the physical to the computational space. We compute the following vectors

$$\boldsymbol{\sigma}_x^{\text{upwind}} = \boldsymbol{w}_{ij} - \boldsymbol{w}_{i-1\,j}, \qquad \boldsymbol{\sigma}_x^{\text{downwind}} = \boldsymbol{w}_{i+1\,j} - \boldsymbol{w}_{ij}, \tag{18}$$

$$\boldsymbol{\sigma}_y^{\text{upwind}} = \boldsymbol{w}_{ij} - \boldsymbol{w}_{ij-1}, \qquad \boldsymbol{\sigma}_y^{\text{downwind}} = \boldsymbol{w}_{ij+1} - \boldsymbol{w}_{ij}, \tag{19}$$

which are used with the minmod limiter implemented in this study. The minmod limiter is defined for two functions a and b as

$$\min\text{mod}\,(a,b) = \begin{cases} a, & \text{if} \quad |a| < |b| \quad \text{and} \quad a \cdot b > 0, \\ b, & \text{if} \quad |a| > |b| \quad \text{and} \quad a \cdot b > 0, \\ 0, & \text{if} \quad a \cdot b < 0. \end{cases} \tag{20}$$

According to the minmod limiter definition (20), we calculate

$$\boldsymbol{\sigma}_x^{\min\text{mod}} = \min\text{mod}\,(\boldsymbol{\sigma}_x^{\text{upwind}}, \boldsymbol{\sigma}_x^{\text{downwind}}), \qquad \boldsymbol{\sigma}_y^{\min\text{mod}} = \min\text{mod}\,(\boldsymbol{\sigma}_y^{\text{upwind}}, \boldsymbol{\sigma}_y^{\text{downwind}}). \tag{21}$$

The reconstructed values on the edges of the control volume Ω_{ij} are evaluated as

$$\boldsymbol{w}_{i+\frac{1}{2}j} = \boldsymbol{w}_{ij} + \frac{1}{2}\boldsymbol{\sigma}_x^{\text{minmod}}, \qquad \boldsymbol{w}_{i-\frac{1}{2}j} = \boldsymbol{w}_{ij} - \frac{1}{2}\boldsymbol{\sigma}_x^{\text{minmod}}, \tag{22}$$

$$\boldsymbol{w}_{ij+\frac{1}{2}} = \boldsymbol{w}_{ij} + \frac{1}{2}\boldsymbol{\sigma}_y^{\text{minmod}}, \qquad \boldsymbol{w}_{ij-\frac{1}{2}} = \boldsymbol{w}_{ij} - \frac{1}{2}\boldsymbol{\sigma}_y^{\text{minmod}}. \tag{23}$$

The total inviscid AUSM numerical flux through the m-th cell edge of the control volume Ω_{ij} is then computed according to equation (17) for

$$\boldsymbol{F}_m^I \equiv \boldsymbol{F}_{L/R}^{AUSM}\left(\boldsymbol{w}_{i+\frac{1}{2}j\,L}, \boldsymbol{w}_{i-\frac{1}{2}j\,R}\right). \tag{24}$$

In order to stabilize the numerical solution in the regions with very low Mach numbers, the following modification of the minmod limiter (20), the so-called ***β-version of the minmod limiter***, has been introduced by the authors

$$\beta - \min\text{mod}\,(a,b) \overset{def}{=} \beta(M) \cdot \min\text{mod}\,(a,b), \tag{25}$$

where the function $\beta(M)$ is chosen as

$$\beta(M) = \begin{cases} 0 & \text{for} \quad M < 0.2, \\ (M - 0.2)/0.8 & \text{for} \quad 0.2 \le M < 1, \\ 1 & \text{for} \quad M \ge 1. \end{cases} \tag{26}$$

This modification of the minmod limiter was proposed particularly for solving of these kinds of transonic flow problems with separation in very narrow channels and gaps.

The approximation of the viscous numerical fluxes $\boldsymbol{F}_m^V$ through the m-th edge ($m = 1,\ldots,4$) of the quadrilateral control volume Ω_{ij} was performed using a finite volume version of central differences on dual cells. For more details, see (Vimmr, 2003).

For the time integration of the ordinary differential equation (10) in semidiscretized form, we use the two stage second order Runge-Kutta algorithm.

5. Experimental method

For the experimental investigation of the clearance flow, a measurement area was designed with embedded 2-D model of the male rotor-housing gap which has the same geometry as in the case of numerical investigation, Fig. 3. The measurement area was attached to the modular wind tunnel of the suction type in the Aerodynamic laboratory of Institute of Thermomechanics ASCR in Nový Knín. Its lower part, which represents the model of the male rotor tooth, was fixed compared to the upper part, which represents the model of the stator. The variable mutual position of both parts enables to change the throat dimension H, Fig. 3. In the performed experimental measurements, four different throat dimensions ($H_1 = 200$ µm, $H_2 = 350$ µm, $H_3 = 500$ µm and $H_4 = 620$ µm) were considered. Both sidewalls of the measurement area have optical windows with the diameter of 160 mm, Fig. 3. The channel width is set to be 20 mm. The total pressure p_{01} at the inlet of the measurement area and the static pressure p_2 near the clearance outlet, Fig. 3, were measured in order to determine the pressure ratio p_2 / p_{01}.

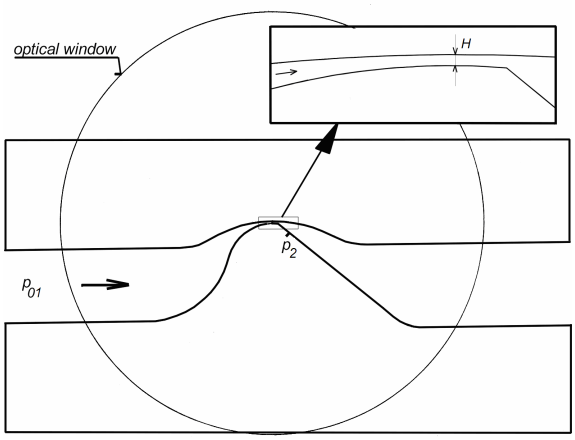

Fig. 3: Designed measurement area with the detail of the male rotor-housing gap

The optical measurement was carried out for four above mentioned throat dimensions ($H_1 - H_4$) and for several selected pressure ratios from the range $0.091 < p_2 / p_{01} < 0.600$ using the Schlieren method in Toepler configuration. For more details regarding the description of this experimental method applied for the investigated clearance flow, see (Luxa et al., 2008).

6. Numerical and experimental results

For the laminar clearance flow computation in all three considered ***test cases A – C***, computational grids were used with refinement in the vicinity of the walls and downstream in the separation region. For example, the structured computational grid for the ***test case A*** with 250×90 quadrilateral cells is shown in Fig. 4.

Regarding the non-dimensional boundary conditions on the boundary $\partial\Omega = \partial\Omega_1 \cup \partial\Omega_2 \cup \partial\Omega_W$ of the computational domain $\Omega \subset R^2$, identical conditions were prescribed for all three test cases at the inlet $\partial\Omega_1$ (the total pressure $p_{01} = 1$, the total temperature $T_{01} = 1$, the inlet angle α_1 of attack of the flow, $\partial T/\partial \boldsymbol{n} = 0$ and $\sum_{k=1}^{2} \tau_{gk} n_k = 0$, $g = 1,2$) and at the rigid walls $\partial\Omega_W$ ($u = 0$, $v = 0$ and $\partial T/\partial \boldsymbol{n} = 0$). The outlet static pressure condition at the boundary $\partial\Omega_2$ is the only exception. For the ***test case A***, the static pressure was set equal to $p_2 = 0.2$, for the ***test case B***: $p_2 = 0.183$ and for the ***test case C***: $p_2 = 0.182$. The other outlet boundary conditions ($\partial T/\partial \boldsymbol{n} = 0$ and $\sum_{k=1}^{2} \tau_{gk} n_k = 0$, $g = 1,2$) are kept the same for all three test cases.

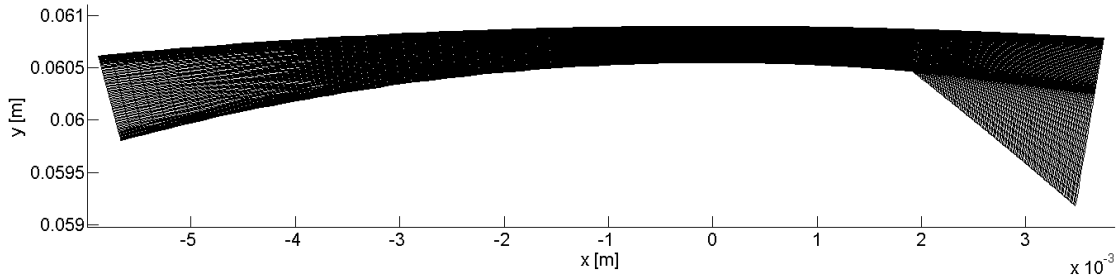

Fig. 4: Structured computational grid for the ***test case A*** (throat dimension $H_2 = 350$ µm) with 250×90 quadrilateral cells

Several obtained numerical and experimental results are presented in Fig. 5 – Fig. 13. The isolines of the Mach number and the velocity magnitude distribution in the 2-D model of the male rotor-housing gap for the ***test case A*** ($H_2 = 350$ µm, $p_2/p_{01} = 0.2$) are shown in Fig. 5 and in Fig. 6. The experimental results visualized in the form of schlieren picture corresponding to this test case are introduced in Fig. 7. The results for the ***test case B*** ($H_3 = 500$ µm, $p_2/p_{01} = 0.183$) and for the ***test case C*** ($H_1 = 200$ µm, $p_2/p_{01} = 0.182$) are presented once again in the form of Mach number isolines, velocity magnitude distributions and schlieren pictures, which can be found in Fig. 8 – Fig. 10 and in Fig. 11 – Fig. 13, respectively.

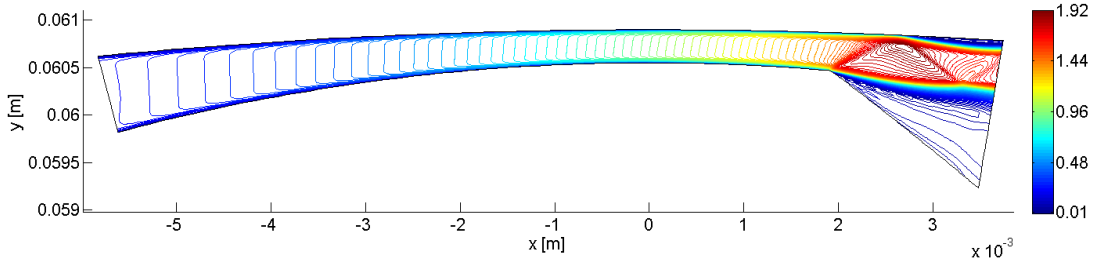

Fig. 5: Isolines of the Mach number for the ***test case A*** ($H_2 = 350$ µm, $p_2/p_{01} = 0.2$)

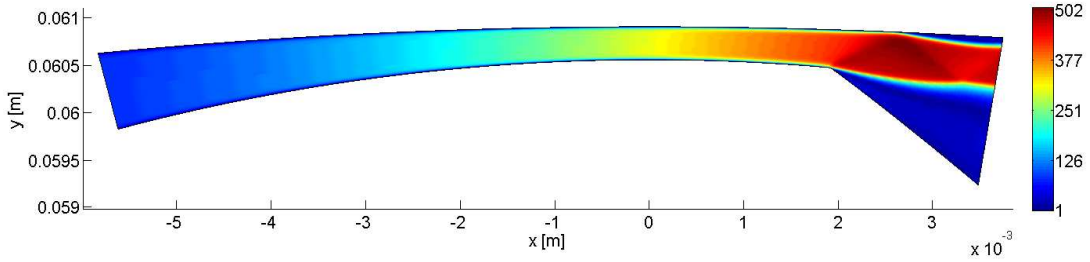

Fig. 6: Velocity magnitude distribution for the ***test case A*** ($H_2 = 350$ µm, $p_2/p_{01} = 0.2$)

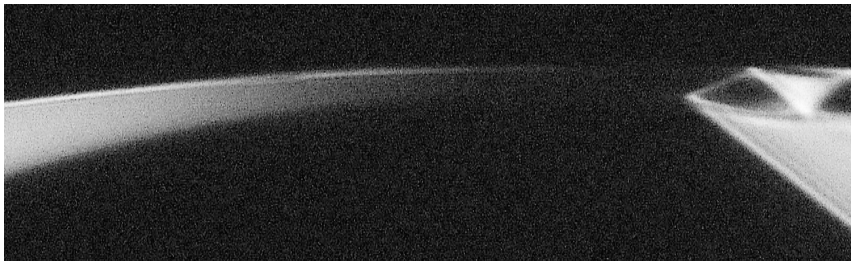

Fig. 7: Schlieren picture for the ***test case A*** ($H_2 = 350$ µm, $p_2/p_{01} = 0.2$)

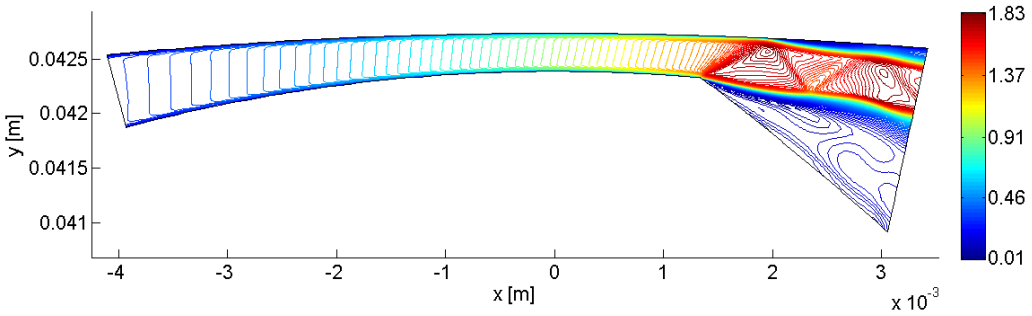

Fig. 8: Isolines of the Mach number for the ***test case B*** ($H_3 = 500$ µm, $p_2/p_{01} = 0.183$)

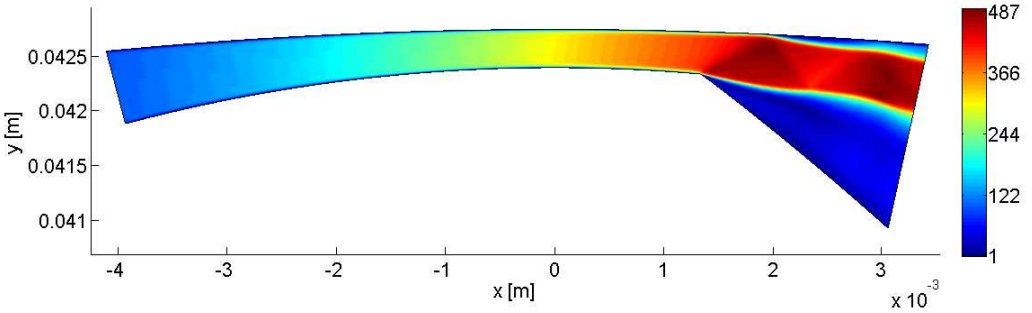

Fig. 9: Velocity magnitude distribution for the ***test case B*** ($H_3 = 500$ µm, $p_2/p_{01} = 0.183$)

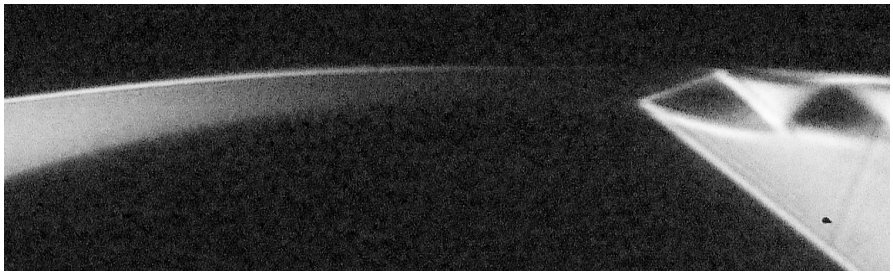

Fig. 10: Schlieren picture for the ***test case B*** ($H_3 = 500$ µm, $p_2 / p_{01} = 0.183$)

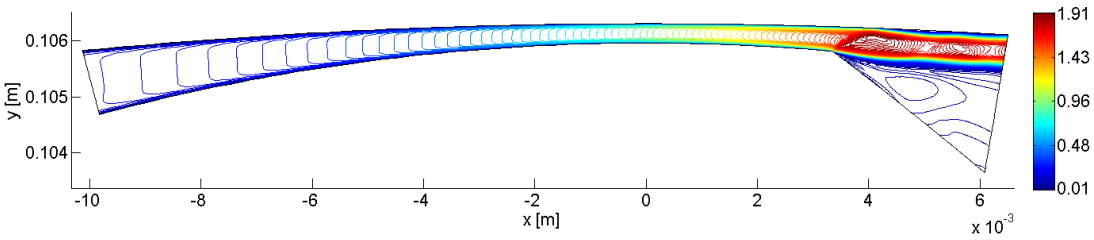

Fig. 11: Isolines of the Mach number for the ***test case C*** ($H_1 = 200$ µm, $p_2 / p_{01} = 0.182$)

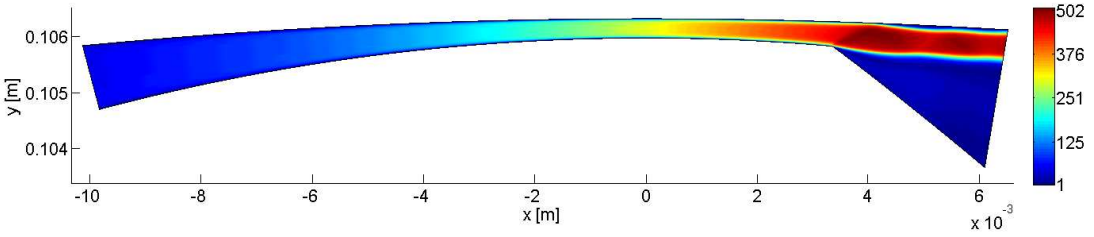

Fig. 12: Velocity magnitude distribution for the ***test case C*** ($H_1 = 200$ µm, $p_2 / p_{01} = 0.182$)

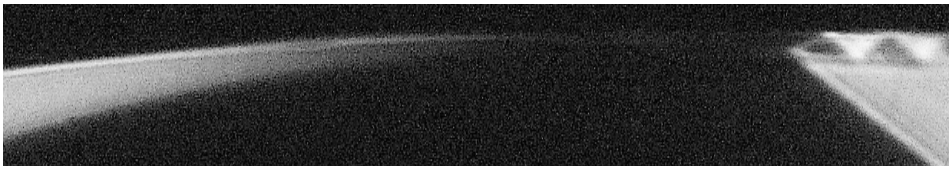

Fig. 13: Schlieren picture for the ***test case C*** ($H_1 = 200$ µm, $p_2 / p_{01} = 0.182$)

7. Conclusions

In regard to the qualitative comparison between the presented schlieren pictures obtained from the experimental measurements, which were carried out in the Aerodynamic laboratory of Institute of Thermomechanics ASCR in Nový Knín, and the numerical results gained by

the developed numerical solver described in this study, it is possible to deduce that both numerical and experimental results are comparable for all our three test cases A – C in the 2-D model of the male rotor-housing gap. Because of the agreement between the numerical and experimental results, we can conclude that the proposed numerical method, which converged to a steady state solution, may be suitable for the solution of transonic flow problems in extremely narrow channels and gaps.

For the considered throat dimensions ($H_1 = 200$ μm, $H_2 = 350$ μm, $H_3 = 500$ μm) of the 2-D model of the clearance gap and for the prescribed pressure ratios ($p_2/p_{01} = 0.182$, $p_2/p_{01} = 0.183$, $p_2/p_{01} = 0.2$), the numerical and experimental results show typical flow field structures. The flow separation area exists not only downstream from the point of the rapid channel area enlargement in the lower part but can be also found near the upper wall as a result of the intensive oblique shock wave incidence.

Acknowledgement

This investigation was supported by the grant GA ČR 101/08/0623 of the Czech Science Foundation.

References

Causon, D. M. (1989) High resolution finite volume schemes and computational aerodynamics. *Notes on Numerical Fluid Mechanics*, vol. 24, pp. 63-74, Vieweg, Braunschweig.

Hirsch, C. (1990) *Numerical computation of internal and external flows*. Fundamentals of numerical discretization – vol. 1. Computational methods for inviscid and viscous flows – vol. 2. John Wiley & Sons, Chichester.

Kauder, K., de Araújo-Rudolph, L. & Sachs, R. (2000) Experimental and numerical investigation of the gas flow using a plane model of male rotor-housing gap in a screw-type machine. *Schraubenmaschinen*, 8, pp. 5-16.

Karniadakis, G., Beskok, A. & Aluru, N. (2005) *Microflows and Nanoflows*. Fundamentals and Simulation – vol. 29 of Interdisciplinary Applied Mathematics.

Liou, M.-S. & Steffen, C. J. (1993) A new flux splitting scheme. *Journal of Computational Physics*, 107, pp. 23-39.

Liou, M.-S. (1996) A sequel to AUSM: AUSM$^+$. *Journal of Computational Physics*, 129, pp. 364-382.

Luxa, M., Dvořák, R., Šimurda, D., Vimmr, J. (2008) Experimental investigation of transonic flow in 2-D model of clearance gap, in: Proc. Conf. Topical Problems of Fluid Mechanics, Institute of Thermomechanics AS CR, Prague, pp. 67-70.

Vimmr, J. (2003) A treatise on numerical computation of non-stationary laminar compressible flow, in: Proc. 19th Conf. Computational Mechanics, University of West Bohemia, Hrad Nečtiny, pp. 483-494.

Vimmr, J. (2004) Mathematical modelling of compressible viscous fluid flow in a male rotor-housing gap of screw machines. *Journal Proc. Appl. Math. Mech.*, 4, pp. 454-455.